Bonding and Reactivity of d^0 Transition Metal Imido Complexes Encoded in their ^{15}N NMR Signatures

Yuya Kakiuchi,[†] Partha Sarathi Karmakar,[‡] Jérémy Roudin,[†] Ian A. Tonks*[,‡] and Christophe Copéret*[,†]

[†] Department of Chemistry and Applied Biosciences, ETH Zürich, Vladimir Prelog Weg 2, CH-8093 Zürich, Switzerland

[‡] Department of Chemistry, University of Minnesota–Twin Cities, Minneapolis, Minnesota 55455, United States

Imido complex, [2+2]-cycloaddition, ^{15}N NMR, solid-state NMR, Electronic structure

ABSTRACT: Terminal imido complexes, containing metal-nitrogen multiple bonds, have been widely used in organometallic chemistry and homogeneous catalysis. The role of terminal imido ligands span from reactive site to spectator motif, largely depending on the nature of the metal center and its specific coordination sphere. Aiming at identifying reactivity descriptors for M-N multiple bonds, we herein explore solid-state ^{15}N NMR spectroscopy (ssNMR) on early-transition metal terminal imido complexes augmented by computaional studies and show that the asymmetry parameter, κ (skew, $1 \geq \kappa \geq -1$), readily available from experiments or calculations, is diagnostic for the reactivity of M-N multiple bonds in imido complexes. While inert imido ligands exhibit skew values (κ) close to 1, highly reactive imido moieties display significantly lower skew values ($\kappa << 1$) as found in metallocene or bis-imido complexes. Natural Chemical Shielding analysis shows that skew values away from 1 are associated with an asymmetric development of π orbitals around the M-N multiple bond of the imido moiety, with a larger double-bond character for reactive imido. Notably, this descriptor does not directly relate to the M-N-C bond angle, illustrating the shortcoming of evaluating bonding and hybridization from geometrical parameters alone. Overall, this descriptor enables to obtain direct experimental evidence for π-loading effect seen in bis(imido) and related complexes, thus explaining their bonding/reactivity.

INTRODUCTION

Terminal imido metal complexes (M=NR) belong to a fundamental class of organometallic compounds, wherein the imido ligand can serve as a stabilizing ancillary ligand or be a key reactive intermediate. These imido ligands can indeed also participate in numerous stoichiometric and catalytic transformations leading to nitrogen-containing compounds, including cycloaddition with unsaturated bonds,[1] nitrene transfer,[2,3] 1,2-addition,[4] or C-H bond activation.[5] Although a wide range of early- and late transition metal imido complexes can be found in catalysis, their reactivity highly depends on the nature of the transition-metal element and the specific structure and electronic configuration, which is often related to the other ligands complementing the coordination sphere of the metal complex. While terminal mono-imido compounds from groups 3- and 4 typically exhibit high reactivity of the imido bond, including [2+2]-cycloaddition with unsaturated substrates, C-H bond activation *etc.*, the reactivity of the imido group significantly drops for later –*e.g.* group 5 and 6– transition-metals, and instead the imido typically finds application as a spectator ligand[6], as exemplified by the ancillary imido ligands in Schrock-type olefin metathesis catalysts.[7,8] Moving further to the right in the Periodic Table, imido complexes of late transition metals again display enhanced reactivity owing to the inherent instability of late transition metal-ligand multiple bonds[9], as elucidated by the "oxo-wall" principle.[10,11] In many instances, the wide range of reactions available to late transition metal imidos hampers their isolation and characterization.

In addition to the effect of metal centre, specific ligand environments are known to enhance the reactivity of the imido ligands. For instance, introduction of strongly π-donating ligands such as additional imido groups (for groups 5 and 6-elements[12–16], or a cyclopentadienyl ligand (mainly for 4-group elements)[17–20] also boosts the reactivity of the imido ligand, in a concept known as the π-loading effect.[12,21] While these reactivity patterns have attracted research interest leading to extensive studies both from experimental and theoretical aspects, no general descriptor of reactivity for the metal-nitrogen bond has been uncovered, and *a priori* prediction of reactivity remains a challenge.

Solid-state NMR (ssNMR) may offer in this regard an ideal platform to link reactivity patterns observed across transition metal imido complexes to specific spectroscopic signatures.[22,23] ssNMR enables measuring each principal component of the chemical shift tensor – δ_{11}, δ_{22} and δ_{33} ($\delta_{11} \geq \delta_{22} \geq \delta_{33}$/ppm) – and thereby the related asymmetric parameters such as span (Ω, eq. 2) and skew (κ, eq. 3) and offers the possibility to build a molecular orbital picture linking chemical shift to electronic structure and reactivity (eq. 1 and Fig. 1). While chemical shift (δ) is observed experimentally with respect to a reference compound, chemical shielding (σ, eq. 4) is an intrinsic property of nuclei in their local environment and accessible by

calculations. This shielding value can be decomposed into diamagnetic (σ_{dia}) and paramagnetic plus spin-orbit ($\sigma_{para+SO}$) terms (eq 5).

$$\delta_{iso} = \frac{1}{3}(\delta_{11} + \delta_{22} + \delta_{33}) \quad (1)$$

$$\Omega = \delta_{11} - \delta_{33} \quad (2)$$

$$\kappa = 3(\delta_{22} - \delta_{iso})/\Omega \quad (3)$$

$$\delta_{ii} = \sigma_{iso}^{ref} - \sigma_{ii} \; (i = 1, 2 \text{ or } 3) \quad (4)$$

$$\sigma = \sigma_{dia} + \sigma_{para+SO} \quad (5)$$

$$\sigma_{para,ij} = -\frac{1}{2c^2}\sum_n \sum_k \frac{1}{E_n - E_0} \langle \Psi_0 | \hat{L}_{k,i} | \Psi_n \rangle \left\langle \Psi_n \left| \frac{\hat{L}_{k,j}}{r_k^3} \right| \Psi_0 \right\rangle \quad (6)$$

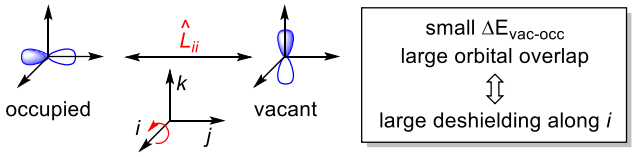

Figure 1. Magnetically induced coupling of occupied and vacant orbitals leading to a deshielding along the *i*-axis.

These terms originate from an isotropic screening and shielding of the nuclei by electrons (σ_{dia}), and an anisotropic component associated typically with deshielding ($\sigma_{para+SO}$), which arises mostly from the frontier molecular orbitals (eq. 6).[24,25] While σ_{dia} is usually constant across a broad range of molecular structures for a given nucleus, $\sigma_{para+SO}$ often plays a pivotal role in driving the NMR chemical shifts, being mostly influenced by the nature (symmetry) and the energy of frontier molecular orbitals, thus opening the possibility to connect NMR signature to reactivity.[22,23] According to the Ramsey equation (eq. 6), deshielding is driven by magnetically coupled occupied and vacant orbitals of appropriate symmetry (orthogonal to each other and to the direction of the applied magnetic field), which can be identified by Natural Chemical Shift (NCS) analysis (Figure 1).[26,27] Recent studies have demonstrated the potential of ^{13}C Chemical Shift Tensor (CST) analysis as a tool to assess the electronic structure and understand the reactivity of metal-carbon bonds in transition metal alkyl-, alkylidene and alkylidyne species towards metathesis, dimerization and polymerization, exploiting the metal-carbon π-interaction as a key parameter that describes reactivity.[23,28–32] Considering the rather large chemical shift window of ^{15}N NMR (>1000 ppm) and the relative ease of ^{15}N-labeling of the imido ligand, analysis of ^{15}N chemical shift tensors of transition metal imido complexes could allow an assessment of their electronic structure and thereby create the opportunity to possibly directly tie spectroscopic signature to reactivity. In fact, besides solution-NMR studies,[33,34] a few available examples of ^{15}N ssNMR draw the potential of such approach. For instance, pioneering ^{15}N ssNMR studies on molybdenum imido and nitrido complexes shows that the axially symmetric spectral pattern was indicative of *sp*-hybridization on M≡NR fragment.[35] More recently, the technique was applied to actinoid-nitrogen multiple bonds to interrogate their covalency.[36–38]

In this work, we employ ^{15}N ssNMR to probe the electronic structure of a number of early transition metal imido complexes, with the goal to rationalize their reactivity patterns and evaluate chemical shift, a readily available parameter, as a descriptor of reactivity. We herein focus on a prototypical reaction, [2+2] cycloaddition with alkynes, because of its prominence as a primary step for numbers of organic transformation and because its concerted mechanism allows us to concentrate on imido-centered reactivity and avoid complex multi-step processes. The solid-state ^{15}N NMR spectra of these imido complexes are highly sensitive towards the imido electronic structure and reveal a diagnostic reporter in the degree of anisotropy of the chemical shift: skew (κ, eq 3), which is directly related to the magnitude of each chemical shift tensor principal components and related to the N-hybridrization. Natural chemical shielding (NCS) analysis identifies that the development of anisotropy resulting from interaction of the two possible π(M-N) orbitals defines the reactivity of the imido ligand, highlighting the role of specific ligand set/geometry on imido-centered transformation.

RESULTS

Solution ^{15}N NMR studies. In an effort to evaluate the possible relation between ^{15}N NMR chemical shift and reactivity, a family of early transition metal imido complexes was selected covering 4-6 group metals with various reactivity profiles toward [2+2] cycloaddition with alkynes in which the presence of filled, high-lying π(M-N) orbital as well as vacant, low-lying π*(M-N) orbital holds the key. The compounds investigated can be divided in several classes: (i) group 5-6 mono-imido halides, which are typically unreactive; along with three classes that are reactive toward cycloaddition: (ii) group 4 mono(imido) halide complexes; (iii) group 5/6 bis(imido) complexes; and (iv) group 4 metallocene imido complexes (Summarized in Figure 2).

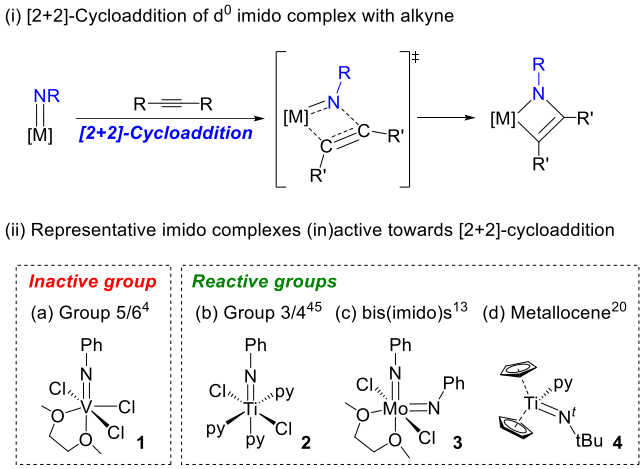

Figure 2. (i) [2+2]-cycloaddition of imido complexes and alkyne. (ii) The complexes focused in this study, representing imido ligand as (a) spectator motif in group 5-6 mono(imido) complexes, and reactive sites in (b) group 3-4 mono(imido), (c) group 5-6 bis(imido) and (d) metallocene imido complexes.

To initiate our investigation, the solution-state ^{15}N NMR chemical shift was first examined (Table 1). The relevant ^{15}N NMR chemical-shifts were obtained using ^{1}H-^{15}N HSQC experiments without a need of labelling on imido nitrogen (Figure S2-S9). Among the series, we could not identify the general trend in the observed ^{15}N chemical shift (δ_N) against either their reactivity, or the M-N-C bond angle which is often used to discuss the hybridization on the imido ligand.[33] For instance, V(=NPh)Cl_3(dme), representing a rather unreactive group 5 mono(imido) complex, displays a δ_N of 498 ppm, similar to what is observed for Mo(=NPh)$_2Cl_2$(dme) (δ_N = 470 ppm) and Cp_2Ti(=N^{t}Bu)(py) (δ_N = 483 ppm), both of which exhibit high reactivity for the imido moiety. In contrast, another highly reactive bis(imido) complex W(=NDipp)$_2Cl_2$(dme) resonates at δ_N = 407 ppm, which is the most shielded value among the series. These results have prompted us to record solid-state ^{15}N NMR spectra of the series in order to measure the principal components of the chemical shift tensor, and thereby the anisotropy of the signal related to the detailed electronic structure.

Solid-state ^{15}N NMR studies. Because solid-state ^{15}N NMR suffers from inherent insensitivity arising from significant broadening of the NMR signal due to the anisotropy and associated spinning side band manifold, four selected ^{15}N-labelled complexes were synthetized –V(=^{15}NPh)Cl_3(dme) (**1$_{15N}$**), Ti(=^{15}NPh)$Cl_2(py)_3$ (**2$_{15N}$**), Mo(=^{15}NPh)$_2Cl_2$(dme) (**3$_{15N}$**) and Cp_2Ti(=^{15}N^{t}Bu)(py) (**4$_{15N}$**) (For synthetic details, see ESI), and their solid-state ^{15}N MAS NMR spectra recorded. These compounds were then used to benchmark our computational approach, thereby enabling the extraction of the electronic structure of each compound (For fitting details, see ESI).

Table 1. Solution-state ^{15}N NMR chemical shift and experimental M-N-C angle on selected imido complexes.

Compound	δ_N[a] (ppm)	M-N-C (°)(ref. No.)
Ti(NPh)$Cl_2(py)_3$ (**2**)	413[b]	177[39]
Ti(N^{t}Bu)$Cl_2(py)_3$	462	172[40]
V(NPh)Cl_3(dme) (**1**)	498	179
Mo(NPh)Cl_4(thf)	453	175[41, c]
W(NPh)Cl_4(thf)	434	177[42]
Cp_2Ti(N^{t}Bu)(py) (**4**)	483	161[19]
Mo(=NPh)$_2Cl_2$(dme) (**3**)	470	162 [d]
W(=NDipp)$_2Cl_2$(dme)	407	164[43, d]

[a] δ_N were obtained by ^{1}H-^{15}N HSQC experiment in C_6D_6 or [b]thf-d_8 at 500 MHz spectrometer. Chemical shift relative to liquid NH_3. [c] Value from *p*-tolyl(imido) analogue. [d]Average value of M-N-C angles in crystal structure.

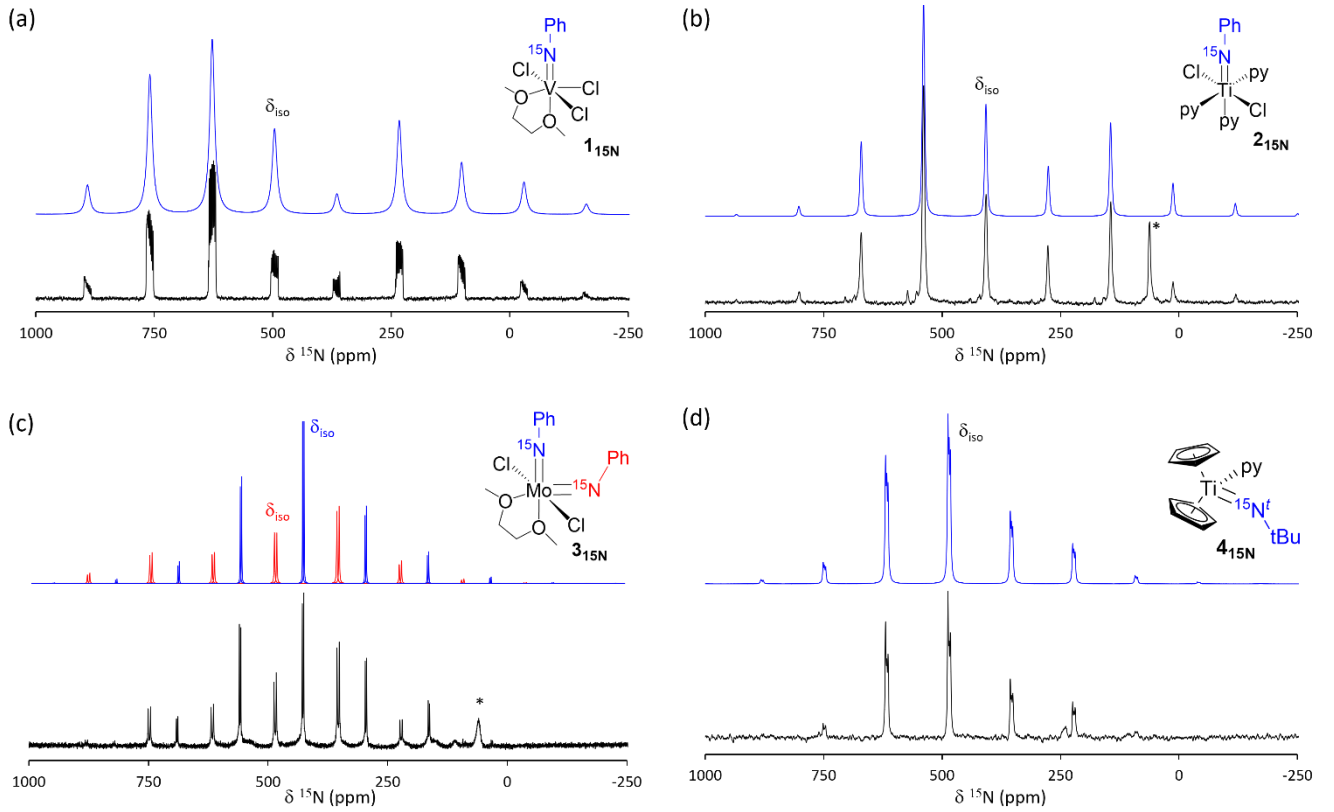

Figure 3. Experimental ^{15}N CP-MAS NMR spectra (black), and simulation (blue/red) of (a) V(=^{15}NPh)Cl$_3$(dme) (**1$_{15N}$**), (b) Ti(=^{15}NPh)Cl$_2$(py)$_3$ (**2$_{15N}$**), (c) Mo(=^{15}NPh)$_2$Cl$_2$(dme) (**3$_{15N}$**) and (d) Cp$_2$Ti(=^{15}N^{t}Bu)(py) (**4$_{15N}$**). All spectra were collected at 8k Hz MAS at 600 M Hz spectrometer. Decomposition product (^{15}N-aniline) were denoted with asterisk (*).

The experimentally obtained solid-state ^{15}N MAS NMR spectra for **1$_{15N}$** -**4$_{15N}$** are shown in Fig. 3. ^{15}N-labelled V(=^{15}NPh)Cl$_3$(dme) (**1$_{15N}$**) exhibits an axial spectral pattern with two strongly deshielded components, δ_{11} = 787 ppm and δ_{22} = 782 ppm, vs. δ_{33} = -81 ppm, giving δ_{iso} = 496 ppm with an axial skew value κ = 0.98 (Fig. 2a). The coupling of ^{15}N with neighboring ^{51}V nuclei (spin=7/2, 99.8% natural abundance) results in an octet for each side band with $^1J_{VN}$ = 135 Hz. A similar signature was observed for the group 4 mono(imido) analogue, Ti(=^{15}NPh)Cl$_2$(py)$_3$ (**2$_{15N}$**) exhibiting κ = 0.99. (figure 3b). This highly axial solid-state ^{15}N chemical shift pattern was similarly reported for cationic molybdenum(VI) imido or neutral nitrido complexes.[35] Such spectral signatures are typically observed for axially symmetric (ca. C_∞ axis) environments, as found in the ^{13}C solid-state NMR spectra of alkynes and transition metal alkylidyne complexes.[44] This is indeed consistent with the structure of these mono-imido species featuring essentially linear M-N-C angles, pointing to *sp*-hybridized nature of the nitrogen (table 1). While common spectral features are observed for **1$_{15N}$** and **2$_{15N}$**, they have contrasting reactivity: while **1** is inert towards cycloaddition with alkyne[14], **2** has been known as a potent catalyst for [2+2+1]-pyrrole formation reaction which involves [2+2]-cycloaddition process as a key step.[45] This difference will be addressed in later section.

Group 6 bis(imido) complexes have been employed as a reactive center in catalytic/stoichiometric transformations, in contrast to the unreactive mono(imido) analogues.[13,46] The two imido fragments in bis(imido) species often appear to be inequivalent in the solid state;[47] this is also true for Mo(=NPh)$_2$Cl$_2$(dme) (**3**) as revealed by single-crystal X-ray diffraction analysis (Figure S1). While one of the imido moieties has shorter Mo-N length (1.704/1.744 Å for 2 molecules in an asymmetric unit, respectively, and the same hereafter) as well as larger Mo-N-C angle (167.5/175.5 °), the other imido ligand has significantly longer Mo-N distance (1.757/1.755 Å) with a smaller Mo-N-C angle (151.7/151.5 °). These structural deviations suggest their different hybridization on nitrogen; the linear imido moiety can be described as *sp*-hybridized nitrogen while bent imido ligand has *sp*^{2}-character. In fact, ssNMR spectroscopy highlights the contrasting signature for these two groups. Although solution state ^{15}N NMR gave single signal for **3** implying the rapid interconversion of these imido ligands (Table 1), solid-state ^{15}N NMR of **3$_{15N}$** successfully captured the difference of these imido moieties (Figure 3c). Each sideband has a "doublet-like" splitting, which can be attributed to the two distinct molecules in an asymmetric unit in the crystal. Since each pair of "doublets" has a similar spectral parameter, their average is used in the discussion hereafter (For full extraction of the spectrum and fitting, see ESI). The extracted parameters allow for decomposition of the spectrum into two distinct signals showing isotropic chemical shifts at 485 ppm and 427 ppm both of which feature a significantly low skew value: κ = -0.54 and 0.27, respectively, contrasting to that of mono(imido) analogues. In fact, such a low skew value combined with a large span draws parallels to the solid-state ^{13}C NMR spectra of transition metal alkylidene complexes,[44] implying significant double-bond character of the N=M bond within these species. Combined with geometrical parameters, the signal at 485 pm

(κ = -0.54, Ω = 728 ppm) is assigned to the bent-imido moiety, while the one at 427 ppm (κ = 0.27, Ω = 560 ppm) is assigned to the linear imido ligand, although such a low skew value is unexpected from its geometrical linearity. These assignments were further corroborated by DFT calculations based on the crystal structures (*vide infra*).

Lastly, ^{15}N ssNMR spectrum for the titanocene imido complex $Cp_2Ti(=^{15}N^tBu)(py)$ (**4_{15N}**) was reported in Figure 3d, representing the reactive group 4 metallocene imido family. The spectrum of **4_{15N}** contains 3 species with similar overall parameters, which we assign to potential crystal polymorphs. Consistent with this assignment, the solution-state ^{15}N NMR collapses into a single species. For this discussion, the average parameters of the 3 signals was used. The isotropic chemical shift of **4_{15N}** is 485 ppm with a moderately asymmetric signature (κ = 0.45, Ω = 651 ppm) showing the intermediate feature between mono- and bis(imido) complexes.

DISCUSSION

Chemical Shift Tensor Orientations. The experimental investigations reveal the high sensitivity of solid-state ^{15}N NMR towards the chemical—and potentially electronic—environment around the imido nitrogen, primarily modulating its line-shape. While the skew value (κ), which is strongly associated with the position of δ_{22}, is identified a key spectroscopic parameter, the isotropic chemical shift only shows a minor difference among the complexes and is in agreement with the solution-state NMR studies. Since κ is by nature associated to the symmetry around the interested nuclei driven by each principal component, we next looked at the orientation of the calculated ^{15}N chemical shielding tensor (CSTs) and carried out a NCS analysis[26,27] for each complex based on their computed structure and NMR signatures in order to further understand the observed trends. The calculations were first benchmarked against experimental values, showing good correspondence to observations (Table 2).

Table 2. Calculated solid-state ^{15}N NMR parameters. Experimental values are shown in parentheses.

Compound	δ_{iso}	Ω (ppm)[a]	skew (κ)[b]
1_{15N}	513 (496)	1026 (939)	0.94 (0.98)
2_{15N}	440 (407)	716 (728)	0.86 (0.99)
$3_{15N\ linear}$	453 (427)	544 (560)	0.16 (0.27)
$3_{15N\ bent}$	521 (485)	687 (728)	-0.46 (-0.54)
4_{15N}	556 (485)	647 (651)	0.47 (0.45)

[a] Span (Ω) = δ_{11}-δ_{33}. [b] Skew (κ) = 3(δ_{22}-δ_{iso})/(δ_{11}-δ_{33}).

The visualized orientations of the CSTs of **1-4** are summarized in Figure 4a-e. The CST orientations were found to be common among the herein investigated imido complexes. The most and second-most deshielded tensor components, δ_{11} and δ_{22}, are oriented perpendicular to the M-N bond, while the most shielded δ_{33} is more along the bond. Such orientations are analogous to isoelectronic transition metal alkylidyne species[44] implying *sp* hybridization around the nitrogen atoms, while the spectral signature (e.g. skew value) significantly differs among the series. Deviation from this general alignment, which could be found in **3_{bent}** and **4**, potentially implies a modulation in the electronic structure for these species (*vida infra*). For bis(imido) complex **3**, the deshielded δ_{11} is perpendicular to the Mo-N bond pointing parallel with N-Mo-N plane for both the linear- and bent imido ligands, whereas δ_{22} points orthogonal to the plane. Similarly, δ_{11} in metallocene species **4** points to Cp ring, *i.e.* another π-donor, while δ_{22} is on the metallocene wedge plane.

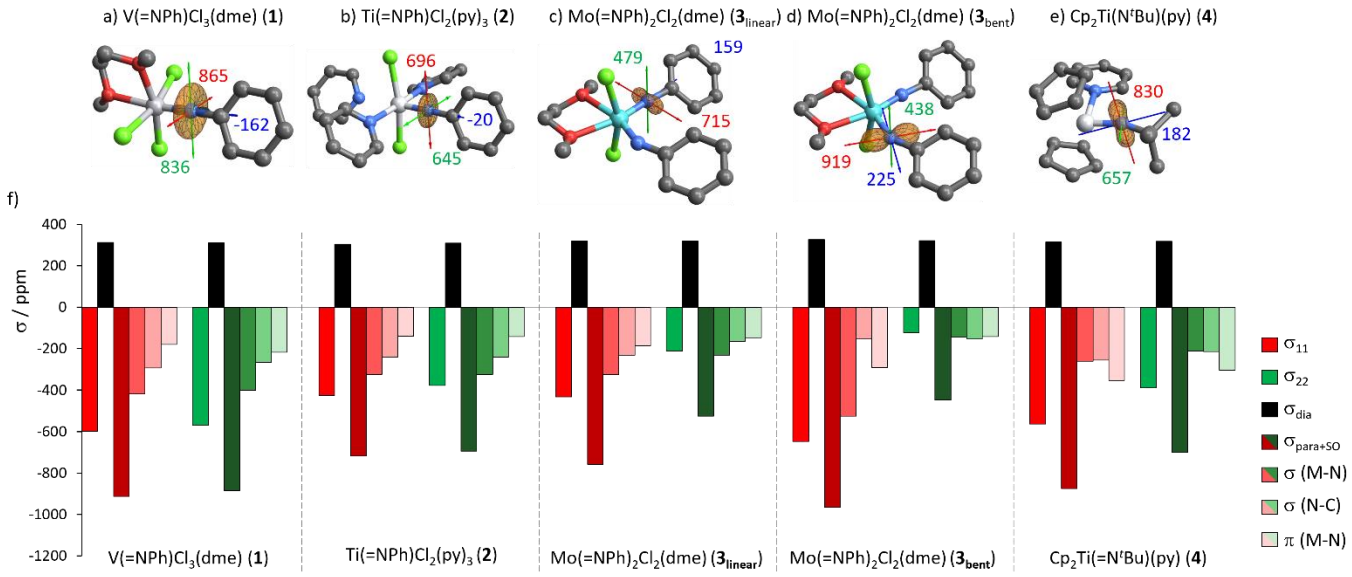

Figure 4. Visualized orientations of CSTs in (a) V(=NPh)Cl_3(dme) (**1**), (b) Ti(=NPh)Cl_2(py)$_3$ (**2**), (c) The linear imido ligand for Mo(=NPh)$_2Cl_2$(dme) (**3**$_{linear}$), (d) the bent imido ligand for Mo(=NPh)$_2Cl_2$(dme) (**3**$_{bent}$) and (e) Cp_2Ti(=N^{t}Bu)(py).). Orientations of $\delta(\sigma)_{11}$, $\delta(\sigma)_{22}$ and $\delta(\sigma)_{33}$ are shown in red, green, and blue arrows, respectively. The ^{15}N NMR chemical shift values (δ) are indicated in ppm next to the direction of each principal component. (f) Summary of NCS analysis for σ_{11} and σ_{22} for **1**-**4**

Natural Chemical Shift – NCS – Analysis. We next carry out an NCS analysis in order to identify the respective orbital contributions to each of the principal components of **1**-**4**, and the results for σ_{11} and σ_{22} are summarized in Figure 4f (for σ_{33}, see Figure S23). Coming back to the Ramsey equation (eq. 6), the chemical shielding can be divided into two parts: the diamagnetic (σ_{dia}, black bars in Figure 4f) and paramagnetic/spin-orbit terms ($\sigma_{para+SO}$, dark red/green bars). While contribution from σ_{dia} is found to be virtually constant at ca. 310 ppm with minor deviation among the series, σ_{para} significantly differs and drives the entire change of chemical shielding. A closer inspection on $\sigma_{para+SO}$ component allows us to link the NMR signature to specific orbital interactions (Fig. 1 and eq. 6).

Starting with the simplest examples, in both the mono(imido) species V(=NPh)Cl_3(dme) (**1**) and Ti(=NPh)Cl_2(py)$_3$ (**2**) the σ(M-N) orbital is the main driver for both δ_{11} and δ_{22}, while the σ(N-C) and π(M-N) orbitals follow as the second- and third most important contributions. The large deshielding perpendicular to M-N axis, originating from the σ-orbitals, indicates couplings with two low lying π^*(M-N) orbitals oriented perpendicular to the M-N bond by symmetry (Figure 5a). The similar values of deshielding in the σ_{11}/δ_{11} and σ_{22}/δ_{22} components indicate a similar extent of coupling (*i.e.* the energy gap between the relevant orbitals), further suggesting that the two pairs of π/π^*(M-N) orbitals have similar energies. This supports the *sp*-hybridized nature of the M-N bond in **1** and **2**, where the two π-orbitals are ideally degenerate as schematically depicted in Figure 5a. This can be further observed in the highly shielded δ_{33} component, in which the NCS analysis reveals the shielding contribution from a filled π(M-N) orbital coupled to another orthogonal filled π(M-N) orbital (Figure S23).

The bis(imido)molybdenum complex (**3**) shows a significantly asymmetric spectral pattern and two non-equivalent imido ligands. This is reflected in NCS analysis shown in Figure 4f with stark contrast in orbital contributions between linear- (**N$_{lin}$**) and bent imido ligand (**N$_{bent}$**). The linear imido ligand (**N$_{lin}$**) has σ(Mo-N), σ(N-C) and π(Mo-N) orbitals as the first, second and third drivers for both the σ_{11} and σ_{22} components. The degree of each of these contributions is similar in both directions; this situation is analogous to mono(imido) halides **1** and **2** implying *sp*-hybridized nature of **N$_{lin}$** in **3**. On the contrary, the bent imido ligand (**N$_{bent}$**) has significantly high contribution from both the σ(Mo-N) and π(Mo-N) orbitals in σ_{11}, whereas these contributions are suppressed in σ_{22}, causing a significant difference between σ_{11}/δ_{11} and σ_{22}/δ_{22} components.

Combined with the visualized CST tensor (Figure 4c, d), the large deshielding in σ_{11} in **N$_{bent}$** suggests the better orbital coupling of both the σ- and π(Mo-N) orbitals, which indicates the presence of a low-lying vacant π^*(Mo-N) as well as a high-lying filled π(Mo-N) orbital in the direction perpendicular to both σ_{11} and M-N bond. On the contrary, the suppressed deshielding contribution from σ- and π(Mo-N) orbitals in σ_{22} suggests inefficient coupling between σ-π^*– and π-σ^*(Mo-N) orbital-pairs within N-Mo-N plane. This is due to the reduced contribution of bent-imido-based orbital in the *in-plane* π(N-Mo-N) orbital, which is dominated by the π-bonding between metal and linear-imido ligand. Such an environment, based on inspection on σ_{11} and σ_{22}, suggests a more double-bond character of imido ligand with increased *sp*^{2}-like nature for **N$_{bent}$**. These analyses can be summarized in a schematic MO diagram as shown in Figure 5b. The linear imido moiety has two π-orbitals in rather similar energy level (similarly to complexes **1**/**2**), which leads to more *sp* character on the nitrogen (Figure 5b. left). On the contrary, the π-orbitals in bent imido have significantly different energy levels rendering a *sp*^{2}-hybridized, double-bond character. This elevated energy level of the filled π-orbital, as well as the lower energy π^* orbital in the bent imido ligand immediately imply its role as frontier orbitals enhancing the reactivity on this moiety, which explains the advantage of d^0 *cis*-bis(imido) fragment as a reactive site.

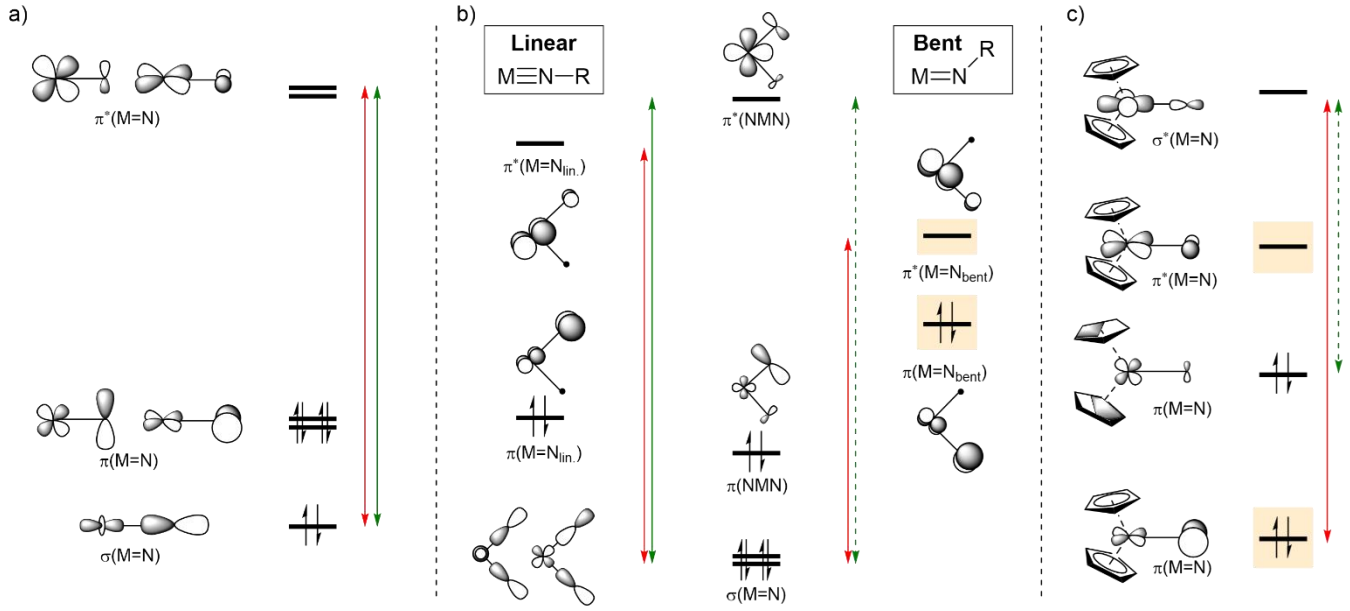

Figure 5. Qualitative MO diagrams of relevant molecular orbitals for (a) mono(imido), (b) bis(imido) and (c) metallocene-imido fragments. Transitions relevant to $\delta_{11}(\sigma_{11})$ and $\delta_{22}(\sigma_{22})$ are indicated with thick red arrows and thin green arrows, respectively. Filled- and vacant orbitals that are relevant to imido-centered reactivity were highlighted in red square.

The large difference between the two CSTs and thus the nature of two π-orbitals can be rationalized in terms of the π-loading effect, or the competitive formation of π-bonds between imido ligands. While each of the two imido ligands is formally capable of forming two π-bonds, there are only three d-orbitals that are allowed by symmetry to participate in such bonding, limiting to a maximum of only three π-bonds. In an extreme depiction, this situation will result in one of the imido ligands forming a triple bond with two π-bonds (*i.e. sp*-hybridization), while the other imido ligand only forming one π-bond (sp^2-hybridization) and thus a strong distortion of the electron density in one specific direction. Such scenario is consistent with the structural differences between the linear and bent imido ligands observed by single crystal diffraction, and further the experimental signature of the ^{15}N ssNMR as well as the NCS analysis. To summarize, competitive π-interactions (π-loading) cause a difference in hybridization around the two imido ligands in bis(imido) complexes; while one of the two imido ligands forms triple bond, and thus is less reactive, the other develops double-bond character with elevated/dropped energy level in the filled π(M-N)/empty π*(M-N) orbital, respectively, offering higher reactivity.

Finally, the metallocene imido species $Cp_2Ti(=N^tBu)(py)$ was investigated in which the π-donating L_2X-type cyclopentadienyl ligand is a potential key player. The experimentally-observed medium skew value (0.45) already indicates the asymmetric orbital development around the imido ligand, which draws contrast to the mono-imido halides **1** and **2**. NCS analysis reveals that the contribution from π(M-N) orbitals is a primary driver in both the δ_{11} and δ_{22} directions, followed by σ(M-N) and (N-C) orbitals as the second- and third- contributors. Combining these observations, the dominant orbital coupling was identified to be π(M-N) to σ*(M-N) along the δ_{11} / δ_{22} axes, and corresponding σ–π* transition follows as the second contributor. A different degree of couplings in the δ_{11} / δ_{22} directions again points to different development of the relevant orbitals in each direction.

The origin of this effect can be rationalized analogously to bis(imido) case, where now the Cp ligands are playing π-competitor role as visualized in the schematic MO diagram in Figure 5c. This π-competition picture is consistent with the well-known analogy between bis(imido) and bent-metallocene fragments.[48] Two Cp ligands in the bent metallocene fragment inherently interact with the d orbital pointing toward

both of the Cp rings; such an orbital further symmetrically matches to one of the π orbitals in imido ligand sitting on Cp-Ti-Cp plane. Although both Cp and imido ligand share the same d orbital, the stronger π-bonding Cp ligands inhibit efficient M-N orbital overlap in this direction, quenching the development of the π(M-N) orbital.[49] In fact, the deshielded δ_{22} component as well as small contribution of this orbital in $\sigma_{para+SO}$ in NCS analysis reflects its Cp-based nature resulting in a poor coupling despite its high-lying energy (indicated as dashed green arrow in Figure 5c). Consequently, only the d orbital in the metallocene wedge position of Cp_2Ti fragment is accessible for π(Ti-N) bond, which results in a double bond between metal and nitrogen, rather than triple bond.

A similar analysis is also conducted on canonical MOs, in order to identify the responsible couplings for deshielding (see detailed discussion for ESI, Figure S29-33), and it is in agreement with the NLMO-based discussion above. The dominant couplings correspond again to filled/vacant pairs of σ-π*/π-σ* transitions among **1**-**4**. To summarize, NCS analysis identified the asymmetric development of π(M-N) orbital as key factor in driving ^{15}N NMR signatures; these results highlight the importance of double-bond character in reactive imido ligand.

Computational Evaluation of Reaction Intermediates.

To this end, one may wonder what the difference between group 4 and 5 imido complexes is: while group 5 mono(imido) complexes are known for their low reactivity, group 4 mono(imido) complexes often exhibit stoichiometric/catalytic reactivity on the imido moiety, yet experimental ^{15}N ssNMR suggests a virtually identical *sp*-hybridized spectral signature of the imido fragments in **1** and **2** (Figure 3a/b, and Figure 4f). In fact, Ti(=NPh)Cl_2(py)$_3$ (**2**) is one of the most potent catalysts for catalytic [2+2+1]-pyrrole formation, which involves [2+2]-cycloaddition[45] as a key step. Envisioning to address the difference between them, we focus on their potential intermediate for [2+2]-cycloaddition upon dissociation of L-type ligands (Figure 6).

While both Ti(=NPh)Cl_2(py)$_3$ and V(=NPh)Cl_3(dme) display a pseudo-octahedral geometry, dissociation of the supported dative ligands (py or dme) yields intermediates with different geometry: trigonal planar for Ti(=NPh)Cl_2 vs. tetrahedral for V(=NPh)Cl_3. The computationally obtained ^{15}N ssNMR parameters for such species suggest a preserved highly axial pattern for V(=NPh)Cl_3 with κ = 0.99 (Figure 6a), while the Ti(=NPh)Cl_2 fragment exhibited lower κ = 0.53 which is indicative to the development of an asymmetric π orbital, *i.e.* partial double-bond character while less significant than bis(imido) case (Figure 6b). The origin of such low skew value is likely due to the Cl ligands: while highly symmetric V(=NPh)Cl_3 fragment has virtually symmetric imido π-bonds, one of the Ti-N π orbitals (parallel to trigonal plane) competes with the Ti-Cl σ bonds quenching its development which results in an asymmetrically developed π orbital perpendicularly aligned to the plane. In addition, removal of an L-ligand from bis(imido) and-metallocene imido complexes **3** and **4** preserves their low skew value ($\kappa < 1$), suggesting they retain their doubly bonded nature in the "naked" state, which is consistent with their high reactivity (Table 3, entry 12, 14). This example illustrates how the κ value can be used as a computational reactivity reporter, offering a facile evaluation methodology for reaction intermediates, which may be otherwise inaccessible.

Finally, to further examine the generality of skew value (κ) as a general reactivity descriptor, the ^{15}N NMR signatures of a series of early transition metal imido complexes were computationally investigated (Table 3). The calculated skew values indeed draw a nice parallel with the reported reactivity of the complex; while inert mono(imido) complexes have higher κ values approaching 1, the cycloaddition-active complexes and intermediates generally have small κ values ($\kappa < 1$) accompanied with lower δ_{22} and higher δ_{33}. Notably, the skew value is independent from the M-N-C angle, which is often conventionally used to discuss the nature of imido bond (see also Figure S20). This further suggests the advantage of using as solid-state NMR parameters to probe the electronic structure and hybridization on imido-nitrogen: crystal packing forces or other steric interactions can play a dramatic role in the stolid-state (*i.e.* single-crystal XRD analysis) M-N-C angle, and thus it is often impossible to deconvolute whether the angle is a result of electronic or simple geometric factors. This can be exemplified by the earlier examples with V(=NPh)Cl_3 and Ti(=NPh)Cl_2 both of which have linear imido moieties (Table 3, entries 10, 11) but very different skew values (0.99 vs. 0.53, respectively) and reactivity.

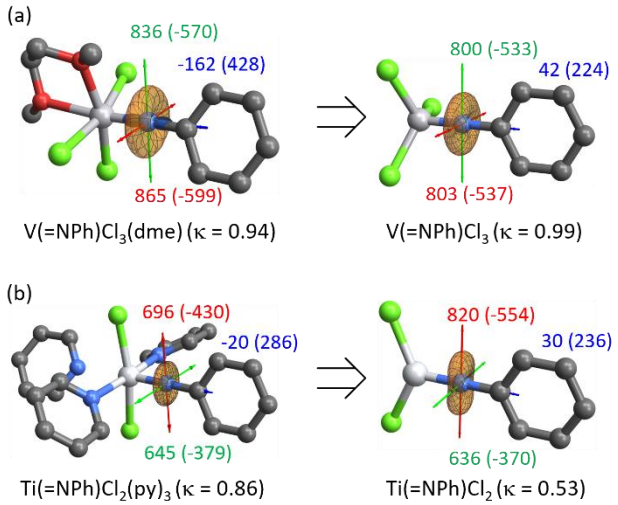

Figure 6. Orientation of the CSTs in (a) V(=NPh)Cl_3(dme) (left)/ V(=NPh)Cl_3 (right) and (b) Ti(=NPh)Cl_2(py)$_3$ (left)/ Ti(=NPh)Cl_2 (right). Calculated ^{15}N NMR chemical shift s (δ) are indicated in ppm next to the direction of each principal component, with the corresponding shielding values (σ) given in parenthesis.

Table 3. Calculated isotropic chemical shifts (d_{iso}), principal components (d_{ii}), skew (κ) and Span (Ω) of the ^{15}N chemical shift tensor for selected transition metal imido complexes and their M-N-C bond angles (°). Experimental d_{iso} values from solution ^{15}N NMR are given in parentheses when available. Cycloaddition-active imido groups (including pre-active species) are shown in red, and inert groups in blue.

Entry	Compound	δ_{iso}	δ_{11}	δ_{22}	δ_{33}	skew (κ)	Ω (ppm)	M-N-C (°)
1	$Ti(NPh)Cl_2(py)_3$[a]	440(413)[d]	696	645	-20	0.86	716	177
2	$V(NPh)Cl_3(dme)$[a]	513 (496)[c]	865	836	-162	0.94	1026	179
3	$Mo(NPh)Cl_4(thf)$[a]	479 (455)[c]	705	675	58	0.91	647	175
4	$W(NPh)Cl_4(thf)$[a]	438 (434)[c]	638	608	68	0.90	569	177
5	$Cp_2Ti(N^tBu)(py)$[a]	556 (483)[c]	830	657	182	0.47	647	161
6	$Cp_2Zr(N^tBu)(py)$[a]	437	628	431	251	-0.05	377	169
7	$V(NPh)_2Cl(PMe_3)_2$[a]	547	995	511	135	-0.12	860	161
8	$Mo(NPh)_2Cl_2(dme)$[b]	460 (470)[c]	756	445	209	-0.14	547	162
9	$W(NDipp)_2Cl_2(dme)$[a]	421 (407)	691	403	170	-0.11	522	165
10	$V(NPh)Cl_3$[b]	548	803	800	42	0.99	761	180
11	$Ti(NPh)Cl_2$[b]	496	820	636	30	0.53	790	180
12	$Cp_2Ti(=N^tBu)$[b]	538	812	510	291	-0.16	521	178
13	$Cp_2Zr(=N^tBu)$[b]	461	729	378	276	-0.55	461	179
14	$Mo(=NPh)_2Cl_2$[b]	471	774	459	179	-0.06	595	160

[a] Initial structure was taken from experimental crystal structures and only H atoms were computationally optimized prior to NMR calculation. [b] Entire structure was optimized prior to the NMR calculation. [c] Value from solution ^{15}N NMR recorded with ^1H-^{15}N HSQC technique in C_6D_6, or [d] THF-d_8.

Similarly, computational removal of supporting pyridine ligand from $Cp_2M(=N^tBu)(py)$ (M = Ti or Zr) (entries 5, 6) yields coordinatively unsaturated $Cp_2M(=N^tBu)$ fragments (entries 12, 13), which are intermediates for [2+2]-cycloaddition reactions. While the computationally-optimized fragments exhibit virtually linear M-N-C angles (178.1 ° for Ti, and 179.4 ° for Zr), the skew value significantly dropped compared to parent complexes (0.47 vs. -0.16 for Ti, and -0.05 vs. -0.55 for Zr), indicating higher reactivity.

Influence of the M-N-C bond angle in imido ligand is further examined by computationally evaluating the effect of bending the imido ligand in $V(=NPh)Cl_3(dme)$ (**1**) on calculated ^{15}N NMR parameters and bond-deformation energy (Figure S22). The result shows that bending the M–N-Ph bond from 176 ° to 157 °, achieving the most "bent" imido ligand in this work, requires only +1.2 kcal/mol.[34,50] Upon bending, the skew value also shows a minor decrease to 0.78 and remains significantly higher than for bis(imido) or metallocene imido complexes, indicating the dominance of electronic effect in driving ^{15}N NMR parameters. The independent nature of ^{15}N NMR parameters from the geometrical structure highlights its strength as a bonding/reactivity descriptor for imido complexes. The facile availability of such parameters, including via simple computational approaches, opens the way to assess the nature of given imido complexes or reaction intermediate which may otherwise be inaccessible, and provides powerful insights into understanding and predicting imido-mediated reactions.

CONCLUSIONS

The solid-state ^{15}N NMR spectroscopic signatures have been identified to be a powerful methodology to assess the electronic structure of transition metal terminal imido complexes. In particular, the skew (κ) value, which is readily available from experiments or DFT calculations, is a powerful diagnostic parameter that gives information about the hybridization and reactivity of the imido ligand. Analysis of the solid-state ^{15}N NMR spectra reveals that axially symmetric spectral signatures with high skew values (κ close to 1) predict inert group 5/6 mono(imido) species, while lower skew values ($\kappa << 1$) are associated with reactive imido ligands, as found in bis-imido and metallocene complexes. NCS analysis indicates that the asymmetric development of the π(M-N) orbitals, *i.e.* hybridization switch from an –inert- triply bonded towards a – reactive- doubly bonded configuration, encodes for reactivity of the imido ligand. Such asymmetry can be achieved by the introduction of an additional ancillary imido ligand or though alternative specific ligand field (bent metallocene). Such situation inhibits the complete formation of π bonds, increasing the double-bond character of the imido and yielding both high-lying filled- and low-lying empty π^* orbitals, hence the increased reactivity of this ligand towards [2+2]-cycloaddition. Importantly, the skew (κ) is shown to be a very good descriptor of this change of hybridization and reactivity, in contrast to the M-N-C angle, which does not provide adequate information on the electronic structure, contrary to expectation. Such readily available NMR parameters, obtained from experiments or computations, offer a simple reactivity descriptor for compounds and reaction intermediates and can thus serve in developing catalysts. As an immediate extension of this work, application of the same strategy on late-transition metal imido complexes is of our interest and will be disclosed in due course.[51,52]

EPILOGUE

"Spectator" Imido Ligand in Schrock-type Olefin Metathesis Catalysts. The analysis of ^{15}N NMR parameters can further highlight the general role of spectator imido ligands in olefin metathesis process, in combination with the complementary ^{13}C NMR parameters, which have been thoroughly discussed in the last decade.[23,30,32,53,54] We have presented above bis(imido) species, in which one triply bonded imido ligand acts as a supporting ligand while the other doubly bonded imido displays increased reactivity. Such a scenario draws parallel with Schrock-type olefin metathesis catalysts (X)(Y)M(=CHR)(=NAr) (M = Mo or W), featuring a spectator imido ligand along with a doubly bonded alkylidene reactive center. The alkylidene moiety has a *sp*^{2}-hybridized carbon clearly lacking the *in-plane* π orbital, hence the imido ligand can be expected to develop its full triply bonded character.[55,56] This is indeed reflected in the calculated ^{15}N NMR parameters for M(=CH^{t}Bu)(=NPh)(O^{t}Bu$_{F3}$)$_2$ (O^{t}Bu$_{F3}$ = trifluoro(*tert*)butyl), which gives skew values of κ = 0.69 and 0.68 for M = Mo and W, respectively. The rather high κ implies the presence of two π(M-N) orbitals of similar energy forming an M-N triple-bond, although it is clear that the presence of the π-donor alkylidene ligand induces an asymmetry around the imido π-bonds. (Fig. 7a). On the other hand, the calculated chemical shift anisotropy pattern of the alkylidene carbon diplays a low skew value (-0.83 for Mo, and -0.57 for W) and reflects the expected more *sp*^{2}-hybridized nature of this ligand. This is indicative of the presence of the high-lying π(M-C) orbital as well as low-lying π*(M-C) orbital, which are consistent with its high reactivity towards [2+2]-cycloaddition with an olefin (Figure 7b, red/brown spectrum). Consequently, despite a decreased skew values in the ^{15}N NMR signature of the imido, the doubly bonded alkylidene ligand dominates the overall reactivity in Schrock-type alkylidene catalyst while the imido ligand behaves as spectator motif. The lack of high-lying M-N π orbital in these metathesis catalysts, which was seen in the bent-imido ligand of bis(imido) complex **3**, is indeed consistent with having a spectator imido ligand during metathesis.

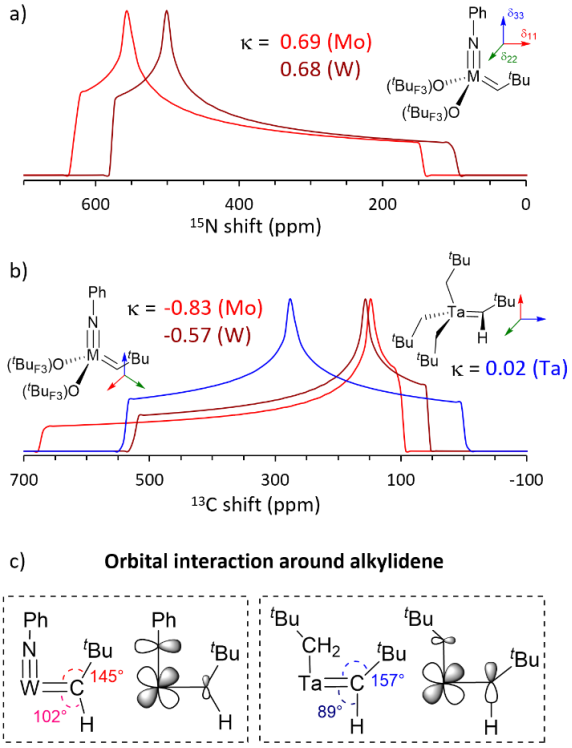

Figure 7. (a) Simulated solid-state ^{15}N NMR chemical shift anisotropy (CSA) pattern for M(=CH^{t}Bu)(=NPh)(O^{t}Bu$_{F3}$)$_2$ (M = Mo (red) or W (brown)). (b) Simulated solid-state ^{13}C NMR CSA pattern for M(=CH^{t}Bu)(=NPh)(O^{t}Bu$_{F3}$)$_2$ (M = Mo (red) or W (brown)) and Ta(=CHtBu)(CH$_2$^{t}Bu)$_3$ (blue). (c) key orbital interaction around alkylidene moiety.

Although such ^{13}C NMR signatures with low skew values are commonly found among the alkylidene ligands of similar Schrock-type alkylidenes,[23,53] the closely related unreactive tantalum alkylidene complex Ta(=CH^{t}Bu)(CH$_2$^{t}Bu)$_3$ exhibits a highly deshielded δ_{22} component with significantly higher ^{13}C skew value (κ = 0.02).[32] This NMR signature indicates the development of M≡C triple-bond character, consistent with a very wide M-C-C bond angle and the presence of an α–H agostic interaction (Figure 7b, blue spectrum).[31] The main origin of the different electronic structure for the alkylidene ligand can be traced back to the availability of an empty d-orbital for additional π-interaction (Figure 7c). While the imido ligand in Schrock-type catalysts occupies the *in-plane* π orbital and forms a triple bond around nitrogen (left), no such *in-plane* π-saturation occurs in Ta(=CH^{t}Bu)(CH$_2$^{t}Bu)$_3$, resulting in an additional low lying d-orbital sitting perpendicular to the Ta-C$_{alkylidene}$ π orbital and able to interact with the p orbitals on carbon (Figure 7c, right), likely explaining the lack of reactivity of this alkylidene. In fact, the presence of the "spectator" imido in Schrock-type metathesis catalysts and bis-imido compounds does not only serve as an ancillary ligand, but also as an activator of the *sp*^{2}-hybridized fragment (M=NR or M=CR$_2$), generating the key reactive site for cycloaddition.[55–57] In other words, the formation of the triple bond around the spectator imido ligand "quenches" the second (potential) π-interaction around the reactive site in the same plane, which promotes the double-bond nature of reactive alkylidene center (*i.e.* a high-lying filled π orbital and low-lying empty π* orbital).

ASSOCIATED CONTENT

The supporting information containing details of synthetic procedure, characterization, NMR experiments and calculations is available in Supporting Information.

AUTHOR INFORMATION

Corresponding Author

Christophe Copéret – Department of Chemistry and Applied Biosciences, ETH Zürich, Vladimir-Prelog-Weg 2, CH-8093 Zürich, Switzerland, Email: ccoperet@ethz.ch

Ian A. Tonks – Department of Chemistry, University of Minnesota–Twin Cities, Minneapolis, Minnesota 55455, United States, Email: itonks@umn.edu

Funding Sources

C.C., Y.K. and J.R. acknowledge the Swiss National Science Foundation (grant numbers 200021_169134, 200020_214994, and 200020B_192050). I.A.T. acknowledges the Swiss National Science Foundation Scientific Exchange Program (IZSEZ0_212682) and National Institutes of Health NIGMS (R35GM119457) for support.

Notes

Any additional relevant notes should be placed here.

ACKNOWLEDGMENT

All simulations were performed on the ETH-Zürich Euler cluster. We thank Dr. René Verel, Dr. Alexander Yakimov and Christoph Kaul for their help with recording solid-state- and solution-state ^{15}N NMR spectra. Teresa Horak is thanked for synthesis of the complex, $W(=NDipp)_2Cl_2(dme)$. Y.K. thanks Sebastian Sabisch for the support regarding the NCS analysis. We acknowledge Dr. Michael D. Wörle (ETHZ) for his assistance in processing the single-crystal XRD data.

ABBREVIATIONS

NMR, nuclear magnetic resonance; ssNMR, solid-state nuclear magnetic resonance; CST, chemical shielding tensor; CSA, chemical shift anisotropy; MAS, magic angle spinning; δ, chemical shift; σ, chemical shielding; Ω, span; κ, skew; XRD, X-ray diffraction; DFT, density functional theory; NCS, Natural chemical shift; Dipp, 2,6-di(isopropyl)phenyl; HSQC, Hetero-nuclear Single Quantum Coherence;

REFERENCES

(1) Kawakita, K.; Parker, B. F.; Kakiuchi, Y.; Tsurugi, H.; Mashima, K.; Arnold, J.; Tonks, I. A. Reactivity of Terminal Imido Complexes of Group 4–6 Metals: Stoichiometric and Catalytic Reactions Involving Cycloaddition with Unsaturated Organic Molecules. *Coord. Chem. Rev.* **2020**, *407*, 213118.

(2) Munhá, R. F.; Zarkesh, R. A.; Heyduk, A. F. Group Transfer Reactions of d^0 Transition Metal Complexes: Redox-Active Ligands Provide a Mechanism for Expanded Reactivity. *Dalton Trans.* **2013**, *42* (11), 3751–3766.

(3) Cosio, M. N.; Powers, D. C. Prospects and Challenges for Nitrogen-Atom Transfer Catalysis. *Nat. Rev. Chem.* **2023**, *7*, 424–438.

(4) Gianetti, T. L.; La Pierre, H. S.; Arnold, J. Group 5 Imides and Bis(Imide)s as Selective Hydrogenation Catalysts. *Eur. J. Inorg. Chem.* **2013**, *2013* (22–23), 3771–3783.

(5) Webb, J. R.; Burgess, S. A.; Cundari, T. R.; Gunnoe, T. B. Activation of Carbon-Hydrogen Bonds and Dihydrogen by 1,2-CH-Addition across Metal-Heteroatom Bonds. *Dalton Trans.* **2013**, *42* (48), 16646–16665.

(6) Anderson, L. L.; Schmidt, J. A. R.; Arnold, J.; Bergman, R. G. Neutral and Cationic Alkyl Tantalum Imido Complexes: Synthesis and Migratory Insertion Reactions. *Organometallics* **2006**, *25* (14), 3394–3406.

(7) Schrock, R. R. Recent Advances in High Oxidation State Mo and W Imido Alkylidene Chemistry. *Chem. Rev.* **2009**, *109* (8), 3211–3226.

(8) Nomura, K.; Zhang, W. (Imido)Vanadium(V)-Alkyl, -Alkylidene Complexes Exhibiting Unique Reactivity towards Olefins and Alcohols. *Chem. Sci.* **2010**, *1* (2), 161–173.

(9) Grünwald, A.; Anjana, S. S.; Munz, D. Terminal Imido Complexes of the Groups 9–11: Electronic Structure and Developments in the Last Decade. *Eur. J. Inorg. Chem.* **2021**, *2021* (40), 4147–4166.

(10) Larson, V. A.; Battistella, B.; Ray, K.; Lehnert, N.; Nam, W. Iron and Manganese Oxo Complexes, Oxo Wall and Beyond. *Nat Rev Chem* **2020**, *4* (8), 404–419.

(11) Gray, H. B.; Winkler, J. R. Living with Oxygen. *Acc. Chem. Res.* **2018**, *51* (8), 1850–1857.

(12) Fostvedt, J. I.; Mendoza, J.; Lopez-Flores, S.; Alcantar, D.; Bergman, R. G.; Arnold, J. Engendering Reactivity at Group 5-Heteroatom Multiple Bonds *via* π-Loading. *Chemical Science* **2022**, *13* (28), 8224–8242.

(13) Lokare, K. S.; Ciszewski, J. T.; Odom, A. L. Group-6 Imido Activation by a Ring-Strained Alkyne. *Organometallics* **2004**, *23* (23), 5386–5388.

(14) Kawakita, K.; Beaumier, E. P.; Kakiuchi, Y.; Tsurugi, H.; Tonks, I. A.; Mashima, K. Bis(Imido)Vanadium(V)-Catalyzed [2+2+1] Coupling of Alkynes and Azobenzenes Giving Multisubstituted Pyrroles. *J. Am. Chem. Soc.* **2019**, *141* (10), 4194–4198.

(15) Fostvedt, J. I.; Grant, L. N.; Kriegel, B. M.; Obenhuber, A. H.; Lohrey, T. D.; Bergman, R. G.; Arnold, J. 1,2-Addition and Cycloaddition Reactions of Niobium Bis(Imido) and Oxo Imido Complexes. *Chem. Sci.* **2020**, *11* (42), 11613–11632.

(16) Helgert, T. R.; Zhang, X.; Box, H. K.; Denny, J. A.; Valle, H. U.; Oliver, A. G.; Akurathi, G.; Webster, C. E.; Keith Hollis, T. Extreme π-Loading as a Design Element for Accessing Imido Ligand Reactivity. A CCC-NHC Pincer Tantalum Bis(Imido) Complex: Synthesis, Characterization, and Catalytic Oxidative Amination of Alkenes. *Organometallics* **2016**, *35* (20), 3452–3460.

(17) Walsh, P. J.; Hollander, F. J.; Bergman, R. G. Generation, Alkyne Cycloaddition, Arene Carbon-Hydrogen Activation, Nitrogen-Hydrogen Activation and Dative Ligand Trapping Reactions of the First Monomeric Imidozirconocene (Cp_2Zr=NR) Complexes. *J. Am. Chem. Soc.* **1988**, *110* (26), 8729–8731.
(18) Blake, R. E.; Antonelli, D. M.; Henling, L. M.; Schaefer, W. P.; Hardcastle, K. I.; Bercaw, J. E. A Cationic Imido Complex of Permethyltantalocene: H_2 and Carbon–Hydrogen Bond Activation, [2 + 2] Cycloaddition Reactions, and an Unusual Reaction with Carbon Dioxide That Affords Coordinated Isocyanate. *Organometallics* **1998**, *17* (4), 718–725.
(19) Dunn, S. C.; Mountford, P.; Robson, D. A. Cyclopentadienyl, Indenyl and Bis(Cyclopentadienyl) Titanium Imido Compounds. *Journal of the Chemical Society, Dalton Transactions* **1997**, No. 3, 293–304.
(20) Manßen, M.; de Graaff, S.; Meyer, M.-F.; Schmidtmann, M.; Beckhaus, R. Direct Access to Titanocene Imides via Bis(H_5:H_1-Penta-Fulvene)Titanium Complexes and Primary Amines. *Organometallics* **2018**, *37* (23), 4506–4514.
(21) Chao, Y. W.; Rodgers, P. M.; Wigley, D. E.; Alexander, S. J.; Rheingold, A. L. Tris(Phenylimido) Complexes of Tungsten: Preparation and Properties of the d^0 W(=NR)$_3$ Functional Group. *J. Am. Chem. Soc.* **1991**, *113* (16), 6326–6328.
(22) Gordon, C. P.; Lätsch, L.; Copéret, C. Nuclear Magnetic Resonance: A Spectroscopic Probe to Understand the Electronic Structure and Reactivity of Molecules and Materials. *J. Phys. Chem. Lett.* **2021**, *12* (8), 2072–2085.
(23) Gordon, C. P.; Raynaud, C.; Andersen, R. A.; Copéret, C.; Eisenstein, O. Carbon-13 NMR Chemical Shift: A Descriptor for Electronic Structure and Reactivity of Organometallic Compounds. *Acc. Chem. Res.* **2019**, *52* (8), 2278–2289.
(24) Kaupp, M.; Bühl, M.; Malkin, V. G. Calculation of NMR and EPR Parameters: Theory and Applications Wiley-VCH Verlag Geinheim. Wiley, 2004; Vol. 128, pp 8987–8988.
(25) Vı Cha, J.; Novotný, J.; Komorovsky, S.; Straka, M.; Kaupp, M.; Marek, R. Relativistic Heavy-Neighbor-Atom Effects on NMR Shifts: Concepts and Trends Across the Periodic Table. *Chem. Rev.* **2020**, *120* (15), 7065–7103.
(26) Bohmann, J. A.; Weinhold, F.; Farrar, T. C. Natural Chemical Shielding Analysis of Nuclear Magnetic Resonance Shielding Tensors from Gauge-Including Atomic Orbital Calculations. *J. Chem. Phys.* **1997**, *107*, 1173-1184.
(27) Autschbach, J. Analyzing NMR Shielding Tensors Calculated with Two-Component Relativistic Methods Using Spin-Free Localized Molecular Orbitals. *J. Chem. Phys.* **2008**, *128* (16), 164112.
(28) Gordon, C. P.; Culver, D. B.; Conley, M. P.; Eisenstein, O.; Andersen, R. A.; Copéret, C. π-Bond Character in Metal-Alkyl Compounds for C-H Activation: How, When, and Why? *J. Am. Chem. Soc.* **2019**, *141* (1), 648–656.
(29) Gordon, C. P.; Shirase, S.; Yamamoto, K.; Andersen, R. A.; Eisenstein, O.; Copéret, C. NMR Chemical Shift Analysis Decodes Olefin Oligo- and Polymerization Activity of d^0 Group 4 Metal Complexes. *Proc. Natl. Acad. Sci. U. S. A.* **2018**, *115* (26), E5867–E5876.
(30) Gordon, C. P.; Yamamoto, K.; Liao, W. C.; Allouche, F.; Andersen, R. A.; Copéret, C.; Raynaud, C.; Eisenstein, O. Metathesis Activity Encoded in the Metallacyclobutane Carbon-13 NMR Chemical Shift Tensors. *ACS Central Science* **2017**, *3* (7), 759–768.
(31) Gordon, C. P.; Yamamoto, K.; Searles, K.; Shirase, S.; Andersen, R. A.; Eisenstein, O.; Copéret, C. Metal Alkyls Programmed to Generate Metal Alkylidenes by α-H Abstraction: Prognosis from NMR Chemical Shift. *Chem. Sci.* **2018**, *9* (7), 1912–1918.
(32) Halbert, S.; Copéret, C.; Raynaud, C.; Eisenstein, O. Elucidating the Link between NMR Chemical Shifts and Electronic Structure in d^0 Olefin Metathesis Catalysts. *Journal of the American Chemical Society* **2016**, *138* (7), 2261–2272.
(33) Bradley, D. C.; Hodge, S. R.; Runnacles, J. D.; Hughes, M.; Mason, J.; Richards, R. L. Nitrogen Nuclear Magnetic Resonance Spectroscopy as a Probe of Bonding, Bending and Fluxionality of the Imido Ligand. *J. Chem. Soc. Dalton Trans.* **1992**, No. 10, 1663–1668.
(34) Ciszewski, J. T.; Harrison, J. F.; Odom, A. L. Investigation of Transition Metal-Imido Bonding in M(NBut)2(Dpma). *Inorg. Chem.* **2004**, *43* (12), 3605–3617.
(35) Sceats, E. L.; Figueroa, J. S.; Cummins, C. C.; Loening, N. M.; Van der Wel, P.; Griffin, R. G. Complexes Obtained by Electrophilic Attack on a Dinitrogen-Derived Terminal Molybdenum Nitride: Electronic Structure Analysis by Solid State CP/MAS ^{15}N NMR in Combination with DFT Calculations. *Polyhedron* **2004**, *23* (17), 2751–2768.
(36) Staun, S. L.; Sergentu, D.-C.; Wu, G.; Autschbach, J.; Hayton, T. W. Use of ^{15}N NMR Spectroscopy to Probe Covalency in a Thorium Nitride. *Chem. Sci.* **2019**, *10* (26), 6431–6436.
(37) Sergentu, D.-C.; Kent, G. T.; Staun, S. L.; Yu, X.; Cho, H.; Autschbach, J.; Hayton, T. W. Probing the Electronic Structure of a Thorium Nitride Complex by Solid-State ^{15}N NMR Spectroscopy. *Inorg. Chem.* **2020**, *59* (14), 10138–10145.
(38) Du, J.; Seed, J. A.; Berryman, V. E. J.; Kaltsoyannis, N.; Adams, R. W.; Lee, D.; Liddle, S. T. Exceptional Uranium(VI)-Nitride Triple Bond Covalency from ^{15}N Nuclear Magnetic Resonance Spectroscopy and Quantum Chemical Analysis. *Nat. Commun.* **2021**, *12* (1), 5649.
(39) Blake, A. J.; Collier, P. E.; Dunn, S. C.; Li, W.-S.; Mountford, P.; Shishkin, O. V. Synthesis and Imido-Group Exchange Reactions Oftert-Butylimidotitaniumcomplexes. *J. Chem. Soc. Dalton Trans.* **1997**, No. 9, 1549–1558.
(40) Collier, P. E.; Dunn, S. C.; Mountford, P.; Shishkin, O. V.; Swallow, D. Dalton Communications. Exchange of Organoimido Groups at a Mononuclear Titanium Centre and a Crystallographic Evaluation of the Relative Structural Influences of the NBut, NC_6H_4Me-4 and $NC_6H_4NO_2$-4 Ligands. *J. Chem. Soc. Dalton Trans.* **1995**, *22*, 3743.
(41) Chou, C. Y.; Huffman, J. C.; Maatta, E. A. An Organoimido Molybdenum(VI) Complex: Preparation and Structure of (p-TolylN)-$MoCl_4$(Thf). *J. Chem. Soc. Chem. Commun.* **1984**, *17*, 1184–1185.
(42) Wright, C. M. R.; Williams, T. J.; Turner, Z. R.; Buffet, J. C.; O'Hare, D. Selective Ethylene Oligomerisation Using Supported Tungsten Mono-Imido Catalysts. *Inorganic Chemistry Frontiers* **2017**, *4* (6), 1048–1060.
(43) Wright, W. R. H.; Batsanov, A. S.; Howard, J. A. K.; Tooze, R. P.; Hanton, M. J.; Dyer, P. W. Exploring the Reactivity of Tungsten Bis(Imido) Dimethyl Complexes with Methyl Aluminium Reagents: Implications for Ethylene Dimerization. *Dalton Trans. J. Inorg. Chem.* **2010**, *39* (30), 7038–7045.
(44) Estes, D. P.; Gordon, C. P.; Fedorov, A.; Liao, W.-C.; Ehrhorn, H.; Bittner, C.; Zier, M. L.; Bockfeld, D.; Chan, K. W.; Eisenstein, O.; Raynaud, C.; Tamm, M.; Copéret, C. Molecular and Silica-Supported Molybdenum Alkyne Metathesis Catalysts: Influence of Electronics and Dynamics on Activity Revealed by Kinetics, Solid-State NMR, and Chemical Shift Analysis. *J. Am. Chem. Soc.* **2017**, *139* (48), 17597–17607.
(45) Gilbert, Z. W.; Hue, R. J.; Tonks, I. A. Catalytic Formal [2+2+1] Synthesis of Pyrroles from Alkynes and Diazenes via Ti(II)/Ti(IV) Redox Catalysis. *Nat. Chem.* **2016**, *8* (1), 63–68.
(46) Tsurugi, H.; Akiyama, T.; Frye, C.; Kakiuchi, Y.; Mashima, K.; Tonks, I. A. Evaluation of Tungsten Catalysis among Early Transition Metals for N-Aryl-2,3,4,5-tetraarylpyrrole Synthesis: Modular Access to N-Doped π-Conjugated Material Precursors. *Inorg. Chem.* **2024**, *63,* 3037–3046.
(47) Barrie, P.; Coffey, T. A.; Forster, G. D.; Hogarth, G. Bent vs. Linear Imido Ligation at the Octahedral Molybdenum(VI) Dithiocarbamate Stabilised Centre. *J. Chem. Soc. Dalton Trans.* **1999**, *0* (24), 4519–4528.
(48) Williams, D. S.; Schofield, M. H.; Schrock, R. R. Synthesis of D2 Complexes That Contain Tungsten [W(NAr)$_2$] and Rhenium [Re(NAr)$_2$] Cores, SCF-X.Alpha.-SW Calculations, and a Discussion of the MCp_2/M'(NR)$_2$ Isolobal Relationship. *Organometallics* **1993**, *12* (11), 4560–4571.

(49) Parkin, G.; Van Asselt, A.; Leahy, D. J.; Whinnery, L.; Hua, N. G.; Quan, R. W.; Henling, L. M.; Schaefer, W. P.; Santarsiero, B. D.; Bercaw, J. E. Oxo-Hydrido and Imido-Hydrido Derivatives of Permethyltantalocene. Structures of $(\eta_5\text{-}C_5Me_5)_2Ta(=O)H$ and $(\eta_5\text{-}C_5Me_5)_2Ta(=NC_6H_5)H$: Doubly or Triply Bonded Tantalum Oxo and Imido Ligands? *Inorg. Chem.* **1992**, *31* (1), 82–85.
(50) Antiñolo, A.; Espinosa, P.; Fajardo, M.; Gómez-Sal, P.; López-Mardomingo, C.; Martin-Alonso, A.; Otero, A. Synthesis and Structural Characterisation of New Isocyanate and Imido Niobocene Complexes. Crystal Structures of $[\{Nb(\eta\text{-}C_5H_4SiMe_3)_2Cl\}_2]$ and $[Nb(\eta\text{-}C_5H_4SiMe_3)_2(=NPh)Cl]$. *J. Chem. Soc. Dalton Trans.* **1995**, No. 6, 1007–1013.
(51) Ray, K.; Heims, F.; Pfaff, F. F. Terminal Oxo and Imido Transition - metal Complexes of Groups 9-11. *Eur. J. Inorg. Chem.* **2013**, *2013* (22-23), 3784-3807.
(52) Grünwald, A.; Goswami, B.; Breitwieser, K.; Morgenstern, B.; Gimferrer, M.; Heinemann, F. W.; Momper, D. M.; Kay, C. W. M.; Munz, D. Palladium Terminal Imido Complexes with Nitrene Character. *J. Am. Chem. Soc.* **2022**, *144* (20), 8897–8901.
(53) Yamamoto, K.; Gordon, C. P.; Liao, W.-C.; Copéret, C.; Raynaud, C.; Eisenstein, O. Orbital Analysis of Carbon-13 Chemical Shift Tensors Reveals Patterns to Distinguish Fischer and Schrock Carbenes. *Angewandte Chemie* **2017**, *129* (34), 10261–10265.
(54) Copéret, C.; Berkson, Z. J.; Chan, K. W.; de Jesus Silva, J.; Gordon, C. P.; Pucino, M.; Zhizhko, P. A. Olefin Metathesis: What Have We Learned about Homogeneous and Heterogeneous Catalysts from Surface Organometallic Chemistry? *Chem. Sci.* **2021**, *12* (9), 3092–3115.
(55) Poater, A.; Solans-Monfort, X.; Clot, E.; Copéret, C.; Eisenstein, O. Understanding d(0)-Olefin Metathesis Catalysts: Which Metal, Which Ligands? *J. Am. Chem. Soc.* **2007**, *129* (26), 8207–8216.
(56) Poater, A.; Solans-Monfort, X.; Clot, E.; Copéret, C.; Eisenstein, O. DFT Calculations of d^0 M(NR)(CHtBu)(X)(Y) (M = Mo, W; R = CPh_3, 2,6-IPr-C_6H_3; X and Y = CH_2tBu, OtBu, $OSi(OtBu)_3$) Olefin Metathesis Catalysts: Structural, Spectroscopic and Electronic Properties. *Dalton Trans.* **2006**, No. 25, 3077–3087.
(57) The related interplay of in-plane π orbitals were previously discussed in detail by Veige *et al.* for a nucleophilic alkylidyne complex supported by tridentate amido ligand: O'Reilly, M. E.; Ghiviriga, I.; Abboud, K. A.; Veige, A. S. A New ONO3- Trianionic Pincer-Type Ligand for Generating Highly Nucleophilic Metal-Carbon Multiple Bonds. *J. Am. Chem. Soc.* **2012**, *134* (27), 11185–11195.